

# Obscuration of Flare Emission by an Eruptive Prominence

Nat GOPALSWAMY<sup>1</sup> and Seiji YASHIRO<sup>1,2</sup>

<sup>1</sup>*Code 671, NASA Goddard Space Flight Center, Greenbelt, MD 20771, USA*

<sup>2</sup>*Department of Physics, The Catholic University of America, Washington DC 20064 USA*

*nat.gopalswamy@nasa.gov; seiji.yashiro@nasa.gov*

(Received ; accepted )

## Abstract

We report on the eclipsing of microwave flare emission by an eruptive prominence from a neighboring region as observed by the Nobeyama Radioheliograph at 17 GHz. The obscuration of the flare emission appears as a dimming feature in the microwave flare light curve. We use the dimming feature to derive the temperature of the prominence and the distribution of heating along the length of the filament. We find that the prominence is heated to a temperature above the quiet Sun temperature at 17 GHz. The duration of the dimming is the time taken by the eruptive prominence in passing over the flaring region. We also find evidence for the obscuration in EUV images obtained by the Solar and Heliospheric Observatory (SOHO) mission.

**Key words:** Sun:prominences Sun: Flares Sun: coronal mass ejections Sun: microwave emission

## 1. Introduction

One of the greatest contributions of the Nobeyama radioheliograph (NoRH, Nakajima et al. 1994) to the study of solar eruptive phenomena is the information on the eruption of filaments and prominences, which are near-surface manifestations of coronal mass ejections (CMEs). Investigations involving Nobeyama prominence eruptions and white-light CMEs have clarified a number of issues and enhanced our understanding of solar eruptions (see e.g., Hanaoka et al. 1994; Gopalswamy and Hanaoka 1998; Gopalswamy et al. 1998; 1996; Hanaoka and Shinkawa, 1999; Hori and Culhane, 2002; Gopalswamy and Thompson, 2000; Gopalswamy et al. 2003a; Kundu et al. 2004; Shimojo et al. 2006; Gopalswamy et al. 2012). By tracking the locations of prominence eruptions as a function of time, it was found that the polarity reversal at solar poles coincided with the times of cessation of high latitude (poleward of 60°) eruptions (Gopalswamy et al. 2003b; 2012). The spatial relationship between prominence

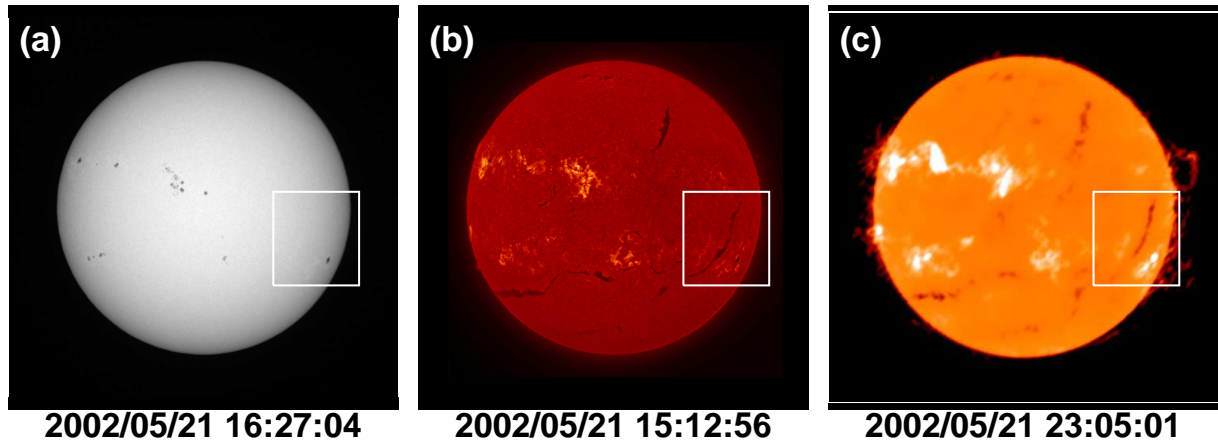


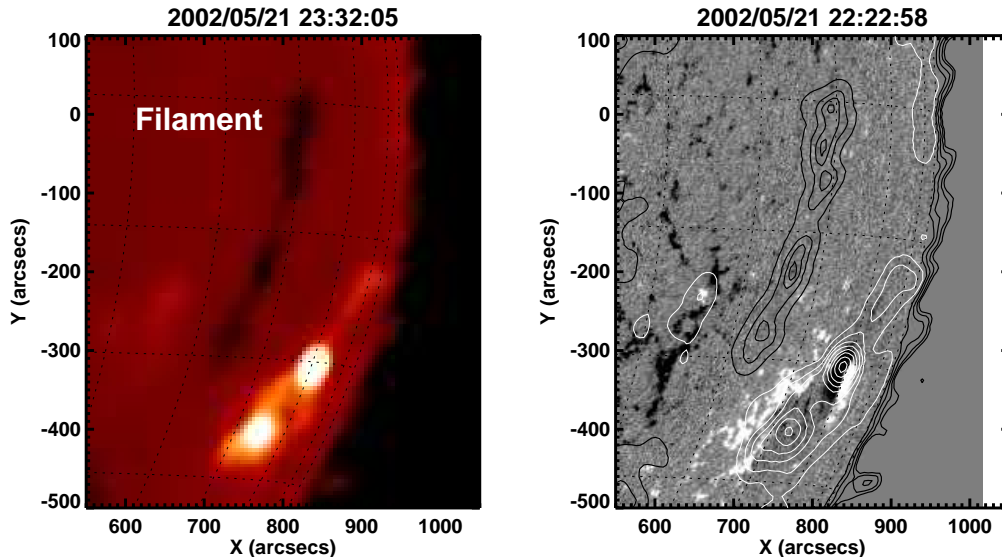
**Fig. 1.** White light 16:27:05 UT (a) and H-alpha at 15:12:56 UT on May 21 (b) images from the Big Bear Solar Observatory, and 17 GHz microwave image from the Nobeyama radioheliograph at 23:05 UT showing the region of interest. The Big Bear H-alpha and white light images show the large sunspot in the negative polarity region of AR 9948.

eruptions and the associated CMEs has also been useful in refining our understanding of CME deflection by coronal holes, especially with respect to the evolution of the poloidal field of the Sun (Gopalswamy et al. 2000; Gopalswamy and Thompson, 2000). In particular, it was possible to show that the position angle of prominence eruptions is systematically offset poleward from the CME position angle during the rise phase of solar cycles (Gopalswamy et al. 2003a; 2012). This offset becomes random in the maximum phase because the polar coronal holes are present only up to the beginning of the maximum phase.

In this paper, we report on another aspect of prominence eruptions: obscuration of neighboring bright flare structure by an eruptive prominence. The observation provides quantitative information on the heating of the prominence during its eruption. We also show that a larger volume of higher optical depth plasma surrounds the eruptive filament.

## 2. Observational Overview

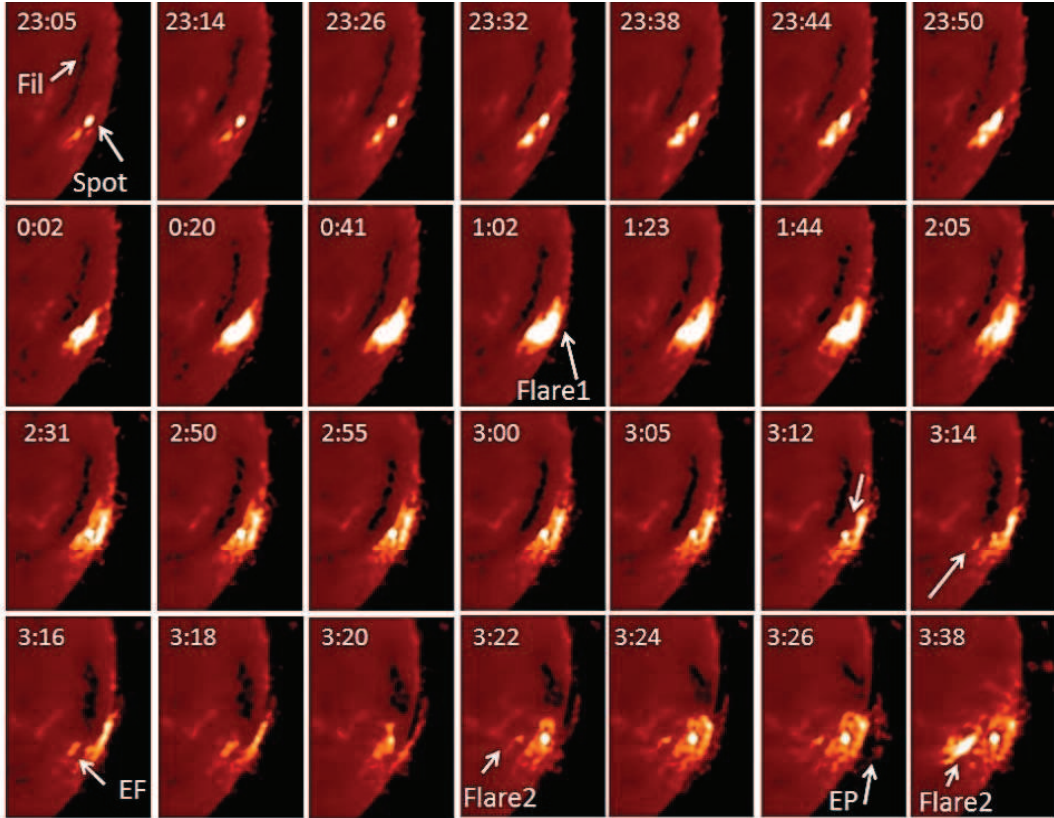
We are concerned about two flares that occurred in the southwest quadrant of the Sun during 2002 May 21-22. The first one was a C9.7 flare from active region NOAA 9948 (S25W64) followed by a C5.0 flare from a neighboring filament region (S30W34). A long quiescent filament, which erupted in association with the C5.0 flare, obscured the preceding flare emission as it passed over it. A partial halo CME with a speed of 1246 km/s was associated with the C9.7 flare, while a full halo CME with a speed of 1557 km/s was associated with the C5.0 flare. The second CME produced an interplanetary type II radio burst and a large solar energetic particle event. Figure 1 shows the region of interest consisting of AR 9948 with a large sunspot (Fig. 1a) and a neighboring filament observed in H-alpha (Fig. 1b) and in microwaves by NoRH (Fig. 1c). The filament extended slightly beyond the lower left corner of the box shown in



**Fig. 2.** Overlay of microwave contours on the SOHO/MDI magnetogram showing Flare1 and the filament. The filament eruption was associated with a spotless flare and a fast CME. The contour levels are 6000, 7000, 8500, 10000, 12000, 15000, 20000, 30000, 50000, 80000, 130000, 180000 K. In the case of the black (white) contours the brightness temperature decreases (increases) towards the peak. The sunspot source has the highest Tb (180,000 K). The southern flare source has a Tb of 130,000 K. The lowest temperature in the filament is 6000 K.

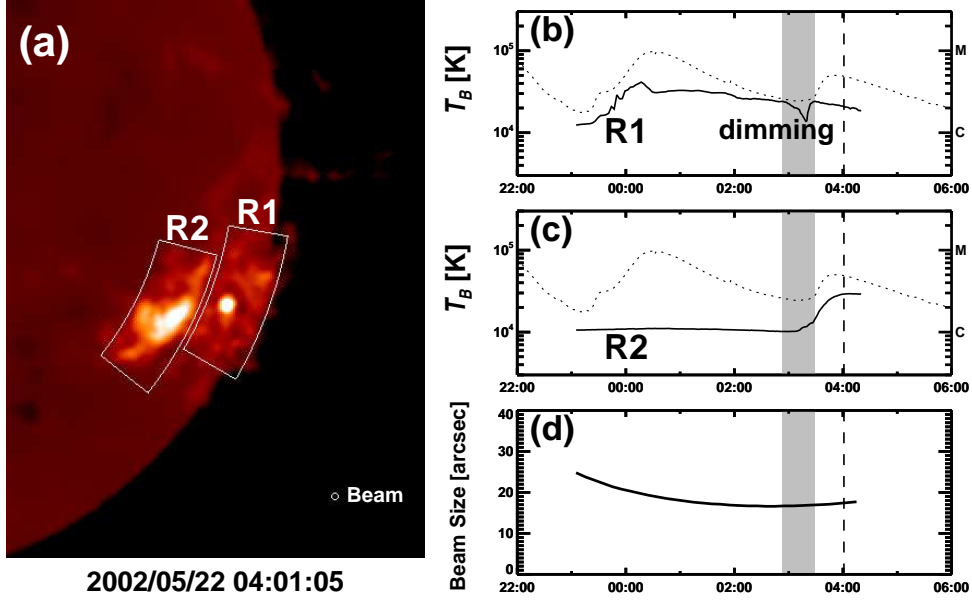
Fig. 1. The filament was located along the neutral line of an extended plage region to the east of AR9948. The sunspot in AR 9948 appears bright in microwaves (Fig.1c) because of the thermal gyroresonance emission due to the high magnetic field above the sunspot located in the negative polarity region. The C9.7 flare, which started, peaked, and ended at 23:14, 00:30, and 01:28 UT, respectively involved the sunspot also.

Figure 2 provides a detailed view of the flaring regions and their magnetic field configuration. The NoRH snapshot at 23:32:05 UT on May 21 was taken about 18 min after the flare onset. The image shows the compact sunspot source at (850,-320) and a new source in the south (770,-400). The brightness temperatures (Tb) of the northern (sunspot) and southern sources were  $1.8 \times 10^5$  K and  $1.3 \times 10^5$  K, respectively. The sunspot source attained a highest Tb of  $4.9 \times 10^5$  K during its peak at 00:17:05 UT on May 22, about 13 min before the flare peak in soft X-rays. The thermal component of the flare was in the form of a post-eruption arcade, which had an average Tb in the range  $2 - 3 \times 10^4$  K (more details in the next section). The thermal emission encompassed the two compact sources and occupied a much larger volume. The filament and the compact sources are shown overlaid as contours on the nearest SOHO/MDI magnetogram taken at 22:22:58 UT on May 21 and rotated to the time of the NoRH image. The two compact sources are on opposite polarity regions. The filament in question divides the opposite polarity regions of the large plage region to the east of the sunspot.



**Fig. 3.** Evolution of the two flares in question (Flare1 and Flare2) along with the eruptive filament from 23:05 UT on 2002 May 21 to 03:38 UT on May 22. The filament (Fil) and the sunspot in the pre-eruption state are marked in the 23:05 UT (May 21) image. The post-eruption arcade of Flare1 is marked in the 01:02 UT (May 22) image. The first instance of significant obscuration by the filament is at the location indicated by the arrow in the 03:12 UT image. In the images at 01:14 and 03:16 UT, the eruptive filament (EF) divides the flare emission into two parts. The flare emission starts recovering from 03:20 UT onwards and the eruptive filament becomes an eruptive prominence (EP) at 03:26 UT. The last image at 03:38 UT shows the post-eruption arcade corresponding to Flare2. The compact source is due to the Sunspot. In microwaves, the sunspots appear bright because of the thermal gyro-resonance emission.

The lowest brightness temperature was  $\sim 6000$  K in the darkest parts of the filament shown in Fig. 2. The quiet-Sun Tb is  $\sim 10^4$  K, corresponding to the level between the highest dark contour ( $10^4$  K) and the lowest white contour ( $1.2 \times 10^4$  K). The second flare started near the southern end of the filament, where the filament had a higher Tb, close to the quiet Sun level. The filament started lifting off slowly around 03:12 UT on May 22 and the soft X-ray flare started around 3:18 UT. The first flare was in the decay phase at this time, but the post eruption arcade was clearly observed in microwaves. The northern leg of the filament remained anchored throughout the eruption. Between 03:12 and 03:24 UT, the eruptive filament passed over the arcade of the first flare causing the dimming we are interested in.



**Fig. 4.** (a) Regions R1 and R2 enclosing microwave flare emission from Flare1 and Flare2, respectively. In the image shown, R1 has the decayed post-eruption arcade from Flare1 and the bright sunspot source. In R2, the bright feature is Flare2. (b,c) Evolution of the flare  $T_b$  from 22:00 UT on 2002 May 21 to 06:00 UT on May 22 in R1 and R2, respectively. The duration of the dimming in (b) is indicated by the gray bar. The GOES light curves of the two flares are shown by the dotted line (the flare intensity level is indicated on the right-side Y-axis). The soft X-ray emission before 23:00 UT is from an unrelated flare in the northeast quadrant. The GOES soft X-ray observation has no spatial information, so the flaring regions cannot be isolated as is done for the microwave emission. The area of the boxes is 1843 pixels ( $2.3 \times 10^{10}$  km<sup>2</sup>). The pixel area is  $4.91 \times 4.91$  ( $5.2 \times 10^5$  km<sup>2</sup>). The vertical dashed line in (b) and (c) marks the time of the NoRH image in (a). In (d), the evolution of the NoRH beam size is shown. The beam size had a constant value of  $\sim 16''.8$  during the time of the obscuration.

### 3. Detailed Evolution of the Two Flaring Regions

Figure 3 shows a series of NoRH images between 23:05 UT on May 21 to 03:38 UT on May 23 illustrating the evolution of the two flares and the eruptive filament eclipsing the microwave emission from the first flare. In the pre-flare state, all we see is the bright sunspot and some plage brightening to the south of the spot (23:08 UT). When the flare started, new compact footpoint sources appeared in the south and at the southern edge of the sunspot (22:32 UT). In the next few minutes, the flare emission appeared in the region between the two compact sources and to the north of the sunspot. Between 00:02 and 01:44 UT, the flare arcade grew in size and the sunspot emission was no longer bright enough to be seen distinctly. When the flare arcade started fading by 02:31 UT, the sunspot emission can be seen again as a compact source. Around 03:05 UT, the southern end of the filament started lifting and by 03:12 UT the eruptive filament (EF) appeared orienting north-south due to the eruption. Even though the EF was still to the east of the flaring region, the flare emission was already



dimmed due to the material surrounding the darkest part of the filament. The dimmed region is pointed by an arrow in the 03:12 UT image. In the next two minutes, the sunspot emission was completely eclipsed by the EF and the flare emission appears divided by the EF. The eastern edge of the flare emission started reappearing after the passage of the EF over it as pointed by an arrow in the 03:14 UT image. In the 03:16 UT image, the EF roughly bisected the flare emission into eastern and western halves. The southern part of the EF was clearly thinner, but much wider over the sunspot. By this time, the EF was in the north-south direction and the darkest part of EF had shortened significantly. Furthermore, the EF appeared much wider than the initial thickness probably because the viewing angle changed due to the moving filament. The maximum obscuration of the flare emission occurred around 03:18 UT. By 03:20 UT, the sunspot emission started emerging from the EF eclipse and by 03:22 UT, most of the flare emission reappeared except for a small section closer to the limb. By 03:24 UT, the entire flare emission reappeared and the EF became eruptive prominence (EP) as it appeared above the limb. NoRH was able to track the EP to much larger distances into the corona and became the core of the fast CME. The second flare (Flare2) associated with the EF became visible as a thin ribbon in the 03:22 UT NoRH image and became the brightest structure by 03:38 UT.

### 3.1. Time profile of the dimming

Figure 4 shows the variation of the brightness temperature in two boxes that enclose the two flaring regions (R1, R2) corresponding to the two flares. The peak Tb in R1 was  $4.1 \times 10^4$  K at 00:17 UT, about 13 min before the soft X-ray flare peak. After this time, the flare emission was mostly from the post-eruption arcade and remained roughly constant at an average Tb of  $2.4 \times 10^4$  K until about 02:53 UT, when the dimming started due to the passage of the eruptive filament over R1. The dimming lasted until about 03:29 UT, when the filament had crossed the flare area and moved above the limb. Thus the dimming lasts for  $\sim 36$  min. At the time of the deepest dimming, the Tb was  $1.4 \times 10^4$  K, which is more than the quiet-Sun Tb. When the dimming ended, the Tb in R1 returned back to the pre-eclipse level ( $2.4 \times 10^4$  K). This also confirms that the eruptive filament was just obscuring the quasi-steady flare emission. Note that the Tb reduction in Fig. 4 is averaged over the area of R1. The flare emission in R2 starts right after the dimming ended in R1 along with the C5.0 flare in GOES soft X-rays.

**Table 1.** Times of deepest dimming and the corresponding Tb in the boxes [b]-[j] in Fig. 5

Time	Tb Min ( $10^4$ K)	Time	Tb Min ( $10^4$ K)	Time	Tb Min ( $10^4$ K)
03:13:05	0.7 [b]	03:17:05	0.9 [c]	03:20:05	0.9 [d]
03:10:05	1.0 [e]	03:17:05	1.1 [f]	03:21:05	1.1 [g]
03:10:05	1.1 [h]	03:17:05	1.5 [i]	03:20:05	1.7 [j]

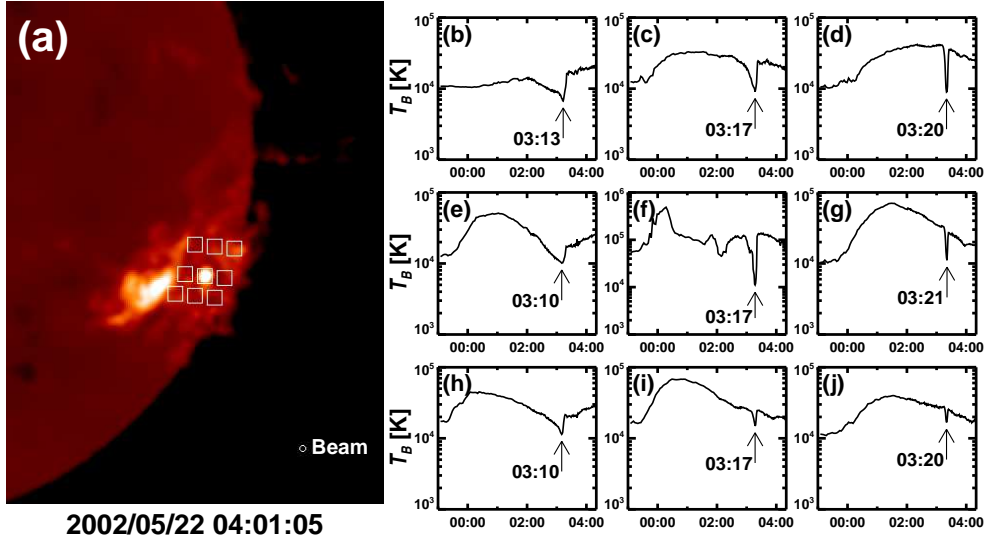


**Fig. 5.** Details of the obscuration at various locations in the flaring region. (a) A NoRH image at 04:01 05 UT with several square boxes overlaid. Each box has a side of 64 pixels ( $2.26 \times 10^5$  km). The NoRH beam around the time of this image is also shown. Time evolution of the brightness temperatures in the nine boxes are shown in the right: (b,c,d) – top row, (e,f,g) – middle row, and (h,i,j) – bottom row. The dimming of the microwave flare emission is marked by arrows including the times when the dimming was the deepest. The Y-axis scale is the same for all plots except for the one in (f) to accommodate the high  $T_b$  in the vicinity of the sunspot. The lower rows are shifted to the east to roughly align with the filament orientation in the beginning. The  $T_b$  increase in boxes (b), (e), and (h) after the dimming is due to the extension of Flare2 emission into these boxes. Table 1. Times of deepest dimming and the corresponding  $T_b$  in the boxes [b]-[j] in Fig. 5.

### 3.2. Spatial Variation of the Flare Obscuration

In order to examine the spatial variation of the flare intensity due to the eclipsing by the eruptive filament, we created 64-pixel boxes within R1 as shown in Figure 5, and tracked the  $T_b$  variation within each of these boxes. Table 1 lists the times of the deepest dimming in each box and the corresponding minimum  $T_b$  values. The times of the deepest minimum is roughly the same for each column and seems progressively later from left to right, tracking the motion of the filament over the flaring region: 03:10 UT in the eastern column (b,e,h), 03:17 UT in the middle column (c,f,i), and 03:20 UT in the western column (d,g,j). The start time of the dimming is not clear in the eastern column because it is located at the edge of the flare arcade. The duration of the dimming ranged from 80 min to 9 min depending on the location. The dimming generally lasted longer in the northern part where the filament and the surrounding structure were larger. The duration of the dimming in the sunspot region was 30 min, similar to the average value in Figure 4. The depth of the dimming essentially depended on the  $T_b$  of the obscuring section of the filament. In the top row of boxes,  $T_b$  dropped to  $0.7 \times 10^4$  K to  $0.9 \times 10^4$  K, remaining below the quiet Sun level. This is also clear from the images in Fig. 3, which shows that the EF remained dark in the north. In the bottom row

of boxes, the Tb dropped to  $1.1 \times 10^4$  K to  $1.7 \times 10^4$  K, which is significantly higher than the quiet-Sun values. In the middle row, the Tb dropped to the quiet Sun value or slightly higher ( $1.0 \times 10^4$  K to  $1.1 \times 10^4$  K). Since the EF completely obscured the flare emission, the observed Tb is the same as the filament Tb. When the filament material is optically thick, the observed Tb is also the kinetic temperature of the filament (see section 5 for a discussion on the optical thickness of the filament). In other words, the filament was heated during the eruption such that the temperature more than doubled in the southernmost part (where the filament lifted off and Flare2 followed). In the middle part, the filament temperature increased by about 50% and in the northern part, the filament temperature changed only marginally. There is also a clear temperature gradient along the axis of the filament, with the highest temperature near the eruption location and the lowest temperature in the northern leg. This is consistent with the fact that the northern leg of the filament remained dark until the filament moved above the limb (see figure 3).

It must be noted that the filament width is larger than the NoRH beam, so the leakage of the bright flare into the beam is negligible. The width of the filament at the thinnest part is  $\sim 62''.8$ . The NoRH beam size (full width at half maximum – FWHM) is  $\sim 16''.8$  (see Figs. 4 and 5). Thus the leakage from the bright flare emission into the Tb of the filament is expected to be very small, especially to at the central part of the filament. The filament Tb at the thinnest part is  $\sim 1.3 \times 10^4$  K. On the east and west edges of the filament, the flare emission had peak values of  $2.3 \times 10^4$  K and  $2.4 \times 10^4$  K, respectively. The deepest part of the filament is at a distance of  $\sim 32''.8$  and  $\sim 30''.0$  from the east and west edges, respectively. By superposing the NoRH beam at these edges (assuming Gaussian), we can see that the leakage from the bright flare emission is negligible. The FWHM of  $16''.8$  implies that the sigma of the beam is  $\sim 7''.1$ . Thus, the deepest part of the filament is 4.6 sigmas away from the east edge, so the leakage component is  $\sim 0.5$  K. Similarly, the leakage contribution from the west edge is  $\sim 3.2$  K. These values are much below the noise level on the maps. The finite size of the beam makes the size of the filament slightly underestimated at the edges.

#### 4. Filament Obscuration in EUV

In this section we present an independent confirmation of the dimming of flare emission in EUV as observed in the images obtained by the Extreme-ultraviolet Imaging Telescope (EIT) on board SOHO. The EIT images were obtained with a low cadence (1 image every 12 minutes). Fortunately, there was one image at 03:12 UT, at which time the dimming clearly was underway. Figure 6 shows three EIT images taken at 03:00 UT, 03:12 UT, and 03:24 UT, roughly corresponding to the pre-dimming, dimming, and post-dimming phases, respectively. The partial obscuration of the EUV arcade emission is clearly seen in the 03:12 UT image and the appearance is very similar to that in the microwave image taken at the same time (see figure 3). In the image at 03:24 UT, the filament had already passed over the flare and appeared



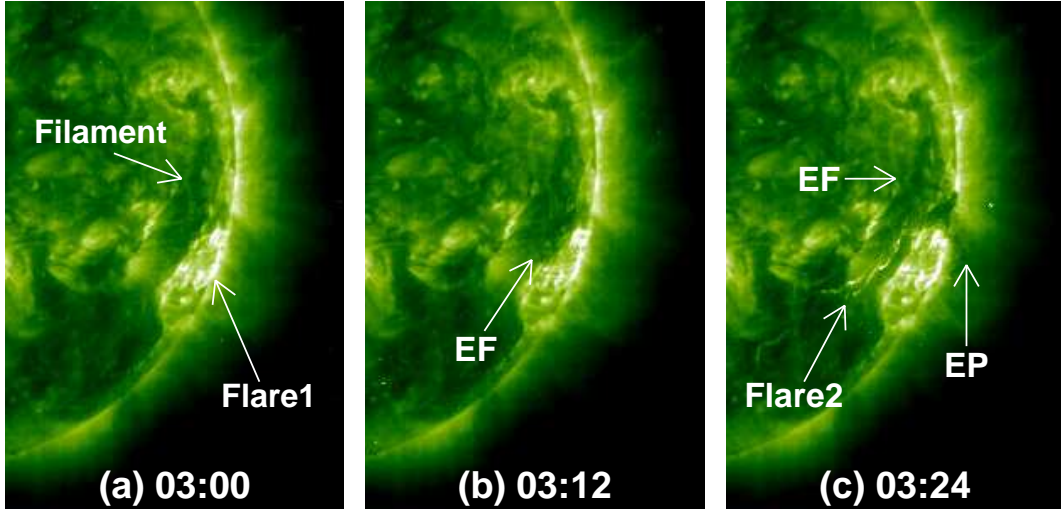


**Fig. 6.** SOHO/EIT images showing the obscuration of the flare emission (Flare1) by the eruptive filament (EF) from the location of the second flare (Flare2). The arrow in the middle panel shows the location where the EF obscured the flare emission. In the right panel, the southern part of the EF moved above the limb and became an eruptive prominence (EP), while the northern leg is still on the disk (EF), similar to what was observed in microwaves.

above the limb. Note that this dimming is due to obscuration by an eruptive filament from a neighboring region and not the usual dimming one observes during the eruption process, due to the evacuation of material on either side of the neutral line. Many eruptive events imaged by the Solar Dynamics Observatory also show the obscuration-type dimming.

## 5. Discussion

In section 3.2 we had assumed that the filament was optically thick. Here we show that the heated filament was optically thick when it was obscuring the flare emission. The radiative transfer equation for the observed brightness temperature can be written as (Dulk, 1985):

$$Tb = \int_0^\tau T_F e^{-t} dt + T_a e^{-\tau}. \quad (1)$$

Here  $T_F$  and  $T_a$  are the physical temperatures of the filament and the flare arcade, respectively;  $\tau$  is the optical depth of the filament. For temperatures  $T < 2 \times 10^5$  K, the absorption coefficient is given by (Webb and Kundu, 1978),

$$\kappa = 0.014gn^2 f^{-2} T^{-3/2} \quad (2)$$

where  $f$  is the observing frequency (17 GHz),  $n$  is the plasma density, and the Gaunt factor  $g$  is given by,

$$g = 18.2 + \ln T^{3/2} - \ln f. \quad (3)$$

For  $T = T_F = 1.3 \times 10^4$  K and  $f = 17$  GHz, we get  $g = 8.8$  and

$$\kappa = 2.9 \times 10^{-28} n^2. \quad (4)$$

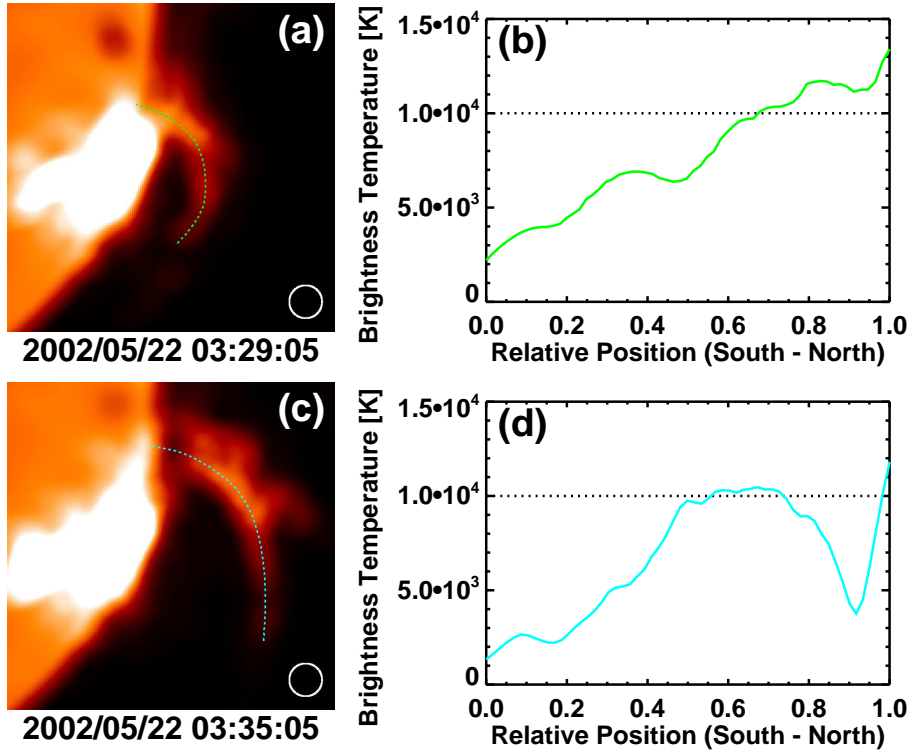


**Fig. 7.** Images of the eruptive prominence at two instances [03:29:05 UT (a) and 03:35:05 UT (c)] with the corresponding brightness temperature variations along the length of the prominence plotted in (b) and (d) from the southern end (position = 0) to the northern end (position = 1). The size of the circle (radius = 8 pixels) that was used in smoothing the images are shown in (a) and (c). Note that some sections of the prominence have brightness temperatures exceeding  $10^4$  K.

Assuming that the line of sight depth  $L$  of the filament is similar to the observed width ( $62''.8$  or  $4.5 \times 10^4$  km), we get the optical depth  $\tau = \kappa L = 1.3 \times 10^{-18} n^2$ . The filament is optically thick if  $n > 8.8 \times 10^8 \text{ cm}^{-3}$ . This inequality is readily satisfied because the density of the pre-eruptive filament is typically  $10^{11} \text{ cm}^{-3}$  and may not be too different in the early phase we are investigating. Irimajiri et al. (1995) found a density of a few times  $10^{10} \text{ cm}^{-3}$  in a few eruptive prominences observed by the 45 m telescope in Nobeyama. We also have independent confirmation of the filament density from white light observations made by the Solar and Heliospheric Observatory (SOHO) mission's Large Angle and Spectrometric coronagraph. A calibrated LASCO image at 04:50 UT was used for this purpose. The eruptive filament became the CME core and was located at a distance of 2.7 Rs from the Sun center. The column density of the prominence material was  $1.3 \times 10^{18} \text{ cm}^{-2}$ . The filament had a width of  $8.6 \times 10^4$  km at the brightest part. Assuming the line of sight depth to be the same as the observed width, we obtained an electron density of  $1.5 \times 10^8 \text{ cm}^{-3}$ . The filament might have expanded and lost mass due to draining before arriving at 2.7 Rs suggesting a reduction in density compared to near-Sun values. Previous estimates have shown that the density decreases by three orders of

magnitude from near the Sun to the coronagraphic FOV (Illing and Athay, 1986). Thus the density of the filament at the time of obscuration is expected to be  $> 10^{10} \text{ cm}^{-3}$ , so we infer that the optical depth  $> 130$ . This result is also consistent with the densities ( $2 - 5 \times 10^{10} \text{ cm}^{-3}$  derived by Irimajiri et al. (1995)). The observed Tb can be explained as a result of heating of the whole filament or the filament with a cool core at  $\sim 8000 \text{ K}$  with an optically thin heated sheath at a temperature of  $\sim 10^5 \text{ K}$  (Hanaoka and Shinkawa, 1999). The sheath needs to be optically thin, contributing a few thousand K to the observed Tb. Note that the second term in eq. (1) drops out due to the large  $\tau$ .

The heating of the eruptive filament is also evident when the filament crossed the limb and became a bright eruptive prominence. Although some sections of the filament might have expanded and became optically thin, the apex part of the prominence probably remained optically thick. We infer this from the observed Tb. Figure 7 shows the Tb variation along two arcs above the limb crossed by the prominence. The arcs are at heliocentric distances of 1.2 and 1.4 Rs in the sky plane. It is clear that some sections of the eruptive prominence had Tb exceeding  $10^4 \text{ K}$ . In order to avoid artifacts in the observed prominence structure (see e.g., Koshiishi 2003), we smoothed the image over circular areas with radius = 8 pixels ( $39''$  or  $2.8 \times 10^4 \text{ km}$ ). Thus the Tb plotted is an underestimate, but confirms that there is definite heating. Let us take the peak value at  $1.2 \times 10^4 \text{ K}$ . The Tb is similar to that of the filament at the time of obscuration. An optically thick filament at  $8000 \text{ K}$  with an optically thin contribution of  $\sim 4000 \text{ K}$  from the heated sheath is consistent with the observations. From equations (2) and (3), we get  $g = 11.9$  and  $\kappa = 1.8 \times 10^{-29} n^2$  for  $T = 10^5 \text{ K}$ . For an average sheath density  $n = 10^9 \text{ cm}^{-3}$ , a sheath thickness of  $\sim 2.2 \times 10^4 \text{ km}$  is needed to account for the optically thin contribution ( $\sim 4000 \text{ K}$ ) from the sheath.

## 6. Summary

The primary result of this paper is that an eruptive filament eclipsed the flare emission for tens of minutes during its transit above the post-eruption arcade in a neighboring active region. The duration of the dimming roughly corresponds to the transit time of the eruptive filament over the neighboring flare. The present observation provides strong evidence that the eruptive filament was heated to temperatures well above that of the quiescent filament. Furthermore, the filament seems to be heated more near the eruption site and progressively less away from the eruption site to almost no heating near the distant leg of the filament. Some sections of the filament remained above  $10^4 \text{ K}$  when the eruptive filament went above the limb as an eruptive prominence. The increased brightness temperature can be explained by a combination of the optically thick emission from the cool filament core and an optically thin emission from the heated filament-corona transition region at a temperature of  $\sim 10^4 \text{ K}$ . The dimming observed is not the one produced as transient coronal holes on either side of the neutral line, but a simple obscuration. The eruptive filament overlies the hot flare plasma and

hence completely eclipsed by the filament. Note that the higher brightness temperature of the flare plasma background made the heated filament visible at microwaves.

Acknowledgement. The authors thank the Local Organizing Committee of the “Solar Physics with Radio Observations” meeting for travel support. The authors benefited greatly from the open data policy of the Nobeyama Solar Observatory and NASA. SOHO is a project of international cooperation between ESA and NASA.

## References

- Dulk, G. A. 1985 *ARA&A*, 23, 169
- Gopalswamy, N., Kundu, M. R., Hanaoka, Y., Enome, S., Lemen, J. R., Akioka, M. 1996 *New Astron.*, 1, 207
- Gopalswamy, N., Hanaoka, Y. 1998 *ApJ*, 498, L179
- Gopalswamy, N., Hanaoka, Y., Lemen, J. R. 1998 *New Perspectives on Solar Prominences*, ed. D. F. Webb, B. Schmieder, and D. M. Rust (ASP Conference Series, Vol. 150, IAU Colloquium 167) p. 358
- Gopalswamy, N., Hanaoka, Y., Hudson, H. S. 2000 *Adv. Space Res.*, 25, 1851
- Gopalswamy, N., Thompson, B. J. 2000 *JASTP*, 62, 1457
- Gopalswamy, N., Lara, A., Yashiro, S., Howard, R. A. 2003a *ApJ*, 598, L63
- Gopalswamy, N., Shimojo, M., Lu, W., Yashiro, S., Shibasaki, K., Howard, R. A. 2003b *ApJ*, 586, 562
- Gopalswamy, N., Yashiro, S., Makela, P., Michalek, G., Shibasaki, K., Hathaway, D. H. 2012 *ApJ*, 750, L42
- Hanaoka, Y. et al. 1994 *PASJ*, 46, 205
- Hanaoka, Y., Shinkawa, T. 1999 *ApJ*, 510, 466
- Hori, K., Culhane, J. L. 2002 *A&A*, 382, 666
- Illing, R. M. E., Athay, A. G. 1986 *Solar Phys.*, 105, 173
- Irimajiri, Y., Takano, T., Nakajima, H., Shibasaki, K., Hanaoka, Y., Ichimoto, K. 1995 *Solar Phys.*, 156, 363
- Koshiishi, H. 2003 *A&A*, 412, 893
- Kundu, M. R., White, S. M., Garaimov, V. I., Manoharan, P. K., Subramanian, P., Ananthakrishnan, S., Janardhan, P. 2004 *ApJ*, 607, 530
- Nakajima, H. et al. 1994 *Proc. IEEE*, 82, 705
- Shimojo, M., Yokoyama, T., Asai, A., Nakajima, H., Shibasaki, K. 2006 *PASJ*, 58, 85
- Webb, D. F., Kundu, M. R. 1978 *Solar Phys.*, 57, 155